AC susceptibility Studies in capped Ni/Ni(OH)$_2$ Core/Shell nanoassemblies: Dual Peak Observations

Jeffrey F. Godsell[1], Tanushree Bala[2], Kevin M. Ryan[2] and Saibal Roy[1*]

[1] *Microsystems Centre, Tyndall National Institute, University College Cork, Lee Maltings, Cork, Ireland.*

[2] *Materials and Surface Science Institute and The Department of Chemical and Environmental Sciences, University of Limerick, Limerick, Ireland.*

* Author to whom correspondence should be addressed,

saibal.roy@tyndall.ie, +353- 21-4904331

Abstract

In the present study, the AC susceptibility (χ` and χ``) variation with temperature (10-100K) for oleic acid capped Ni/Ni(OH)$_2$ core/shell nanoparticle assemblies are reported at frequencies varying from 0.1 Hz to 1000 Hz. Nanoparticle assemblies, with two average particle diameters of ~34 nm and ~14 nm were synthesised using a wet chemical synthesis approach. Two peaks in the AC susceptibility versus temperature curves are clearly discernable for each of the samples. The first, occurring at ~22K was attributed to the paramagnetic/antiferromagnetic transition of the Ni(OH)$_2$ present in the shell. The second higher temperature peak was attributed to the superparamagnetic blocking of the pure Ni situated at the core of the nanoparticles. The higher temperature peaks in both the χ` and χ`` curves were observed to increase with increasing frequency. Thus

the Néel and the blocking temperatures for such core-shell nano-assemblies were clearly identified from the AC analysis, where as they were not discernable (superimposed) even from very low DC (FC/ZFC) field measurements. Interparticle interactions within the assemblies were studied through the fitting of phenomenological laws to the experimental datasets. It is observed that even with an oleic acid capping layer, larger $Ni/Ni(OH)_2$ nanoparticles experience a greater degree of sub-capping layer oxidation thus producing lower magnetic interaction strengths.

I. Introduction

To date magnetic nanoparticles have been successfully synthesised (Godsell et al., 2010, Li et al., 2010, Banerjee et al., 2000, Donegan et al., 2011, Das et al., 2002) and used in a variety of applications such as in magnetic resonance imaging contrasting agents (Huh et al., 2005), ferro-fluids (Gomes et al., 2008), magnetic storage devices (Speliotis, 1999), catalytic applications (Osaka et al., 2008), hyperthermia treatment (Jordan et al., 1999), drug delivery (McGill et al., 2009) etc. The effects of interparticle and surface interactions on magnetic properties has continued to be a central issue in the study of magnetic nanoparticle systems. Interparticle interaction effects between magnetic nanoparticles have previously been analysed through the use of AC susceptibility measurements with the aid of the Néel-Arrhenius and the Vogel-Fulcher laws. In such studies, the frequency of the AC excitation field being applied to the nanoparticles is progressively incremented while the complex susceptibility is measured across a varying temperature range to allow for an exploration of the relaxation processes within the sample.

For the present study, a system of $Ni/Ni(OH)_2$ (core/shell), nanoparticles were analysed. For Ni nanoparticles synthesised within an aqueous environment, it was shown (Bala et al., 2009) that air drying post centrifugation could lead to the

formation of an amount of $Ni(OH)_2$ within the samples. In spite of the presence of an oleic acid (OA) capping layer, a thin shell of $Ni(OH)_2$ was formed, to create a $Ni/Ni(OH)_2$ core/shell type structure. Such a structure allows for an investigation of how the strength of interactions between the particle cores is affected by the presence of a $Ni(OH)_2$ shell around each of the nanoparticles comprising the assemblage. The ability to slightly oxidise the surface of a Ni nanoparticle may be advantageous in certain applications such as in protein separation (Lee et al., 2006), allowing for a tailoring of the sample's magnetic properties. Such effects as a control of magnetisation or the introduction of an exchange bias/pinning effect at lower temperatures are easily achievable with such a core/shell structure. Indeed it has been reported that an exchange bias effect in nanoparticles with antiferromagnetic shells can overcome the superparamagnetic limit, which holds potential interest for the magnetic data storage industry (Skumryev et al., 2003).The potentially interesting control of the magnetic properties allowed by this bilayer $Ni/Ni(OH)_2$ nanostructure were hence deemed worthy of further investigation as detailed in the subsequent sections.

II. Experiment

Details of the particle synthesis technique have previously been reported (Bala et al., 2009). In brief, an aqueous mixture of 1×10^{-2} M $Ni(NO_3)_2 \cdot 6H_2O$ was mixed with 1×10^{-4} M oleic acid and 1×10^{-2} M (sodium dodecyl sulphate) SDS. To produce sample 2 an amount of Pluronic block copolymer (P123) was added to keep the concentration at 0.3% in the solution, however no P123 was added to produce sample 1. The solutions were reduced using 0.035g of $NaBH_4$ in solid form. Post addition of the reducing agent to the solutions the liquid was seen to turn black almost immediately. The solutions were allowed to stand for 30 minutes to ensure the

completion of the reduction reaction before repeatedly being centrifuged at 8000rpm for 15 minutes to separate the pellets. The pellets were then washed using deionised water, the resultant pellets were subsequently dispersed in water. The samples were next fully dried in an air environment to produce a dry powdered sample for magnetic analysis.

The reactions were seen to be perfectly reproducible with the as synthesised particles being reasonably monodisperse. XRD analysis showed the presence of both fcc Ni (PCPDF file no. 04-0850) and $Ni(OH)_2$ in the sample, figure 1. The presence of peaks at 33.8 and 51.5 ensured the hydroxide to be α- $Ni(OH)_2$ (Subbaiah et al., 2003). Figures 2 showed the TEM and HRTEM images of the images of samples 1. A particle distribution analysis (inset, Figure 2A) revealed the size as ~34 nm in diameter. Ni (111) planes could be identified in the HRTEM image (Figure 2C) but no planes for $Ni(OH)_2$ were visible plausibly due to poor crystallinity of the thin hydroxide layers. A detailed XPS analysis (Bala et al., 2009) for the same sample demonstrated fairly good amounts of $Ni(OH)_2$ species. Considering the surface sensitivity of the XPS technique and combining the HRTEM and XPS results, the presence of the hydroxide layers on the surface of the nanoparticles was inferred..

While sample 1 displays particles ~34nm in diameter, sample 2 is seen to be initially bimodal with a small fraction of the particles ~34nm in size but the predominant portion of particles are ~14nm. With sample 2, repeated centrifugation was used to remove the ~34nm particles from the bimodal sample to leave predominantly ~14nm samples behind for magnetic analysis. For both samples, magnetic measurements were performed using a commercial superconducting quantum interference device, (Quantum Design - Model no. MPMS-XL5). For the AC

susceptibility measurements, a peak drive field amplitude of 2.5Oe was applied for all frequencies, no DC offset magnetic field was applied during AC measurement.

III. Theory

With varying AC frequency, the percentage of magnetic nanoparticles which follow the applied field's oscillations will change, inducing an associated modification in the sample's magnetic response. For non-interacting nanoparticle systems, which in turn are subjected to a slowly oscillating magnetic field ($h=h_o\cos\omega_m t$), the real and imaginary parts of the ac susceptibility's components are given by (Singh et al., 2009)

$$\chi' = \chi_o/[1+(\omega_m\tau)^2], \quad (1)$$

$$\chi'' = \chi_o\omega_m\tau/[1+(\omega_m\tau)^2], \quad (2)$$

where $\omega_m = 2\pi f_m$, with $f_m = 1/\tau_m$, the measuring frequency.

The characteristic relaxation time of each particle (τ), attributed to the thermally assisted reversal of the magnetic moments over the anisotropy energy barrier (KV) in the absence of an applied field and which is approximately valid for small applied field strengths is given by a Néel-Arrhenius law (Goya et al., 2003) (Néel-Brown expression (Bedanta and Kleemann, 2009)) as

$$\tau = \tau_0\exp(E_B/k_BT) = \tau_o\exp(KV/\ k_BT). \quad (3)$$

Here V is the particle volume, T is the temperature, K is the effective uniaxial anisotropy, k_B is the boltzmann constant and τ_o is the inverse of the particle attempt frequency ($f_o = \tau_o^{-1}$) which represents the particle's attempt to jump between opposite parallel directions to the magnetisation's easy axis (for superparamagnetic systems typical values of τ_o are ~10^{-9} to ~10^{-11}) (Goya et al., 2003). The blocking temperature (T_B) of the particles, below which the particle's moment will appear frozen on the

time scale of the experiment can be isolated by a rearrangement of equation (3) (with $T = T_B$) as

$$T_B = T_a/\ln(f_0/f_m) \quad (4)$$

where T_a is equal to KV/k_B and $\tau = \tau_m = 1/f_m$. It is known that as the effects of interparticle interactions become increasingly prevalent, then equation (4) will become modified into the form (Singh et al., 2009)

$$T_B = T_a/\ln(f_0/f_m) + T_0 \quad (5)$$

known as Vogel-Fulcher law, where T_0 quantifies the effects of the interparticle interactions. The aforementioned equations are based upon the assumption of uniform particle size. For distributions of particle sizes as in real samples, an average particle size is often assumed as in previous (Singh et al., 2009, Singh et al., 2008) as well as in the present work. For improved accuracy the equations may alternatively be modified appropriately to take account of particle size variation for improved accuracy as previously reported (Gittleman et al., 1974). By fitting the Néel-Arrhenius and the Vogel-Fulcher laws to the measured datasets, the effects of interparticle interactions may be analysed and quantified.

III. Results and Discussion

$Ni(OH)_2$ is an antiferromagnetic material with a bulk Néel temperature of ~26K (Suzuki et al., 2000). While bulk antiferromagnetic materials have a roughly equal numbers of spin-up and spin-down magnetic moments leading to a compensation of the magnetic spins below the material's Néel temperature, on the nanoscale this may not always be true. Nanoscale antiferromagnetic particles may in fact acquire large magnetisations due to uncompensated magnetic spins, such as at the surface. The effects on the magnetic properties of the present samples owing to the presence of $Ni(OH)_2$ may hence be significant.

Figure 4 shows the hysteresis loops of the samples measured at 10K, 30K and 300K. It is seen that at 300K the samples appear to behave paramagnetically, displaying no appreciable coercivity or retentivity. As the temperatures of the samples are lowered to 30K and 10K from 300K, it is seen that the behaviours change from that of a paramagnetic signature to one of a mixed ferromagnetic/paramagnetic type of behaviour. In order to verify if the systems were behaving as ideal superparamagnets, the reduced magnetisations (M/M_s) were plotted as a function of (H/T). The classic law for superparamagnetism dictates that for a pure superparamagnetic sample, the resultant curves would have superimposed onto a universal curve (Knobel et al., 2008). As evident from figure 5, the reduced magnetisation curves did not superimpose thus confirming the prevalence of a more complex underlying mechanism. Additionally, the failure of the samples to fully saturate with increasing field strength even at low temperatures is indicative of the mixed magnetic phases of the sample with the nonmagnetic phase (paramagnetic/antiferromagnetic) failing to achieve saturation even at 50 kOe applied field strength.

In testing for the presence of an exchange bias system, a number of loop shift measurements were conducted. At 300 K, the samples had a magnetic field of 10,000 Oe applied prior to the samples being cooled in the presence of the field down to 5 K. Hysteresis loops were then measured from ± 10,000 Oe. The resulting curves are shown in Figure 6, in the insets of the figures an offset is discernable implying the presence of an exchange bias affect. To facilitate the delineation of the contribution from the different magnetic phases present, AC measurements were employed. To facilitate the further probing of the characteristics of the system, a series of AC susceptibility measurements were carried out at applied AC frequencies of 0.1 Hz, 2.5

Hz, 100 Hz, 500 Hz and 1000 Hz as shown in figure 7. Two peaks were clearly discernable in each of the AC susceptibility measurements at all frequencies. The perfect immobility of the lower temperature peaks with a changing measuring frequency discounts the presence of a blocking temperature at this point in the AC susceptibility measurements. The peaks may plausibly be attributed to the antiferromagnetic Néel temperature of the $Ni(OH)_2$ present in the system. In contrast, it is noted that the position of the higher temperature peaks in both the $\chi`$ and $\chi``$ curves are observed to increase with increasing measurement frequency, a feature characteristic of a superparamagnetic blocking temperature. The peaks in the $\chi$ ($\chi`$ and $\chi``$) versus temperature curves at higher temperatures may hence be attributed to the blocking temperatures of the pure Ni centres at the cores of the core-shell Ni-$Ni(OH)_2$ structures.

In addition to the AC measurements a series of Field-Cooled/Zero-Field-Cooled (FC/ZFC) measurements, with 1 Oe applied field strength were performed on both samples as shown in Figure 8. For both samples, the irreversibility point of the curves were observed at ~22K. A series of additional FC/ZFC measurements at further magnetic field strengths (10 Oe and 100 Oe) were also carried out (not all shown) and produced an similar irreversibility point at ~22K. It is noted that the slight upturn in the ZFC curve of sample 2 was not observed at higher field strengths and as such is likely attributed to the sample settling. The apparent invariance of the temperature of this point with varying applied field strengths appears contrary to what may be expected for a system containing superparamagnetic particles. In such a system it is known that the blocking temperature's position in the ZFC measurement will change with different applied field strengths. This effect has been attributed to the non-linear field of the unblocked particle's magnetisation and has been described

199 elsewhere (Suzuki et al., 2000). As no appreciable changes in the ZFC peak positions
200 were observed with varying applied field strengths, this suggests the possible presence
201 of a Néel temperature without the implication of a blocking temperature at ~22K.
202 However, with the blocking of the nanoparticle assemblages being evidenced in the
203 AC susceptibility measurements, it is therefore likely that these affects are being
204 masked by the Néel temperature peak in the static magnetic measurements. This
205 observed phenomenon may be explained as follows, the blocking temperature can be
206 defined using the following equation (Knobel et al., 2008).

207 $$\ln \tau_m = \ln \tau_0 + \frac{KV_0}{k_B T_B} \quad (6)$$

208 Here it can be seen that T_B is dependent on the measurement time of the
209 experimental apparatus and V_0 is the particle volume. T_B is defined as the temperature
210 at which the characteristic measuring time is equal to the intrinsic relaxation time
211 associated with the nanoparticle's energy barrier. Typically, the measuring time is
212 given a value of 100sec as this is a good approximation for the measurement time
213 scale in a DC magnetometer. With an AC susceptibility measurement, the measuring
214 time will be the inverse of the measurement frequency . In the AC measurements
215 undertaken here, the values of τ_m are therefore 10, 0.4, 0.01, 0.002 and 0.001 for the
216 0.1, 2.5, 100, 500 and 1000 Hz measurement frequencies respectively. The effect of
217 this reduction in the measuring time will be to increase the system's measured
218 blocking temperature from $T_B = \frac{KV_o}{25k_B}$ in the DC case where τ_m = 100 sec and $f_o = 10^9$, to
219 $T_B \approx \frac{KV_o}{14k_B}$ in the AC case where $\tau_m = \frac{1}{1000} = 0.001$. The reduction in the blocking
220 temperatures of the system with increased measuring time for the DC FC/ZFC
221 measurement thus leads to a masking of the blocking temperatures as apparent in
222 Figure 8.

If a simple Néel temperature was being observed at ~22K then the reasons for an irreversibility point in the FC/ZFC curves may not be immediately apparent. It has however additionally been reported that in a mixed ferromagnetic/antiferromagnetic system an irreversibility point in the FC/ZFC curve may also be observed (Acet et al., 2002, Duman et al., 2002). The reasons for this are that for systems with both antiferromagnetic and ferromagnetic materials present, an irreversibility point in the FC/ZFC curves can occur at the lower transition temperature of the two materials present. Be that either the Néel temperature or the Curie temperature, in the present case it occurs at the Néel temperature. The only stipulation for this effect is that the applied field should be sufficiently small. This effect has been attributed to the preferential pinning of the spins into different configurations by the anisotropy of the antiferromagnetic phase. The FC/ZFC measurements can hence be used to determine if different forms of coexisting long range magnetic phases are present in the samples. While the aforementioned effect may be present in the current samples under investigation, the FC/ZFC seperation in figure 8 is sufficiently exaggerated. It is therefore likely that a superposition of both effects (both a pinning at the material boundary and a blocking of the centres) brought about by the coexistence of Ni nanoparticles and a $Ni(OH)_2$ corona is being observed.

It is noted that the particle sizes studied here are below the single domain sizes of Ni (below which the particle becomes a single, uniformly magnetized magnetic domain, as the energy required to create and sustain domain walls is no longer favourable) which are reportedly in the region of ~55 nm (Lu et al., 2007), ~43 nm (Gong et al., 1991). Due to the proximity of the particles, the samples may experience a degree of interparticle interactions. The effect of the capping layer and hydroxide shell will likely be to lessen the likelihood of interactions somewhat by increasing the

inter-core distances. In a real system there are many possible types of interactions which may be present such as exchange interactions, dipole-dipole, tunnelling exchange etc. as outlined by Bedanta et al (Bedanta and Kleemann, 2009).

The degree of interparticle interactions within the two samples is more fully analysed through the use of AC susceptibility measurements. Figure 7 shows the plots of $\chi`$ and $\chi``$, against temperature. The higher temperature's peak positions, were observed to shift to higher temperatures with increased measuring frequencies, an effect also observed in other nanoparticle systems (Shim et al., 2006, Singh et al., 2008, Goya et al., 2003). The frequency dependence of the blocking temperature for isolated particles has been predicted by the superparamagnetic Néel model to follow the Néel-Arrhenius law.

This law (which is equivalent to equation 3) may be expressed in the form (Goya et al., 2003)

$$f = f_o \exp(-T_a/T) \qquad (7)$$

where f is the relaxation frequency ($f=1/\tau$). This law may also be linearised into the equation of a straight line of the form $\ln(f) = (-T_a)(1/T) + \ln(f_o)$ where f is left to equal the measuring frequency f_m, and T is left to equal the blocking temperature T_B. According to G.F.Goya et al, for both the in-phase and the out of phase components of χ, the thermally activated Néel-Arrhenius model is followed. The fitting of this equation to the measured datasets for χ'' is shown in figure 9. The steeper slope of the fitted curve for sample 2 implies that the energy barrier increases from sample 1 to sample 2, this is due to the fact that as the energy barrier E_a is increased then so too does the blocking temperature. It is seen that T_a = 747 K while f_o is 4.11×10^{11}Hz. These values of T_a and f_o can be compared to previously reported values for other Ni nanoparticle systems, a T_a value of 270 K and an f_o of 2.6×10^9 Hz have been reported

for ~ 4nm Ni (~15% loading) nanoparticles also embedded in a nonmagnetic SiO_2 matrix (Singh et al., 2008).

In examining the behaviour of sample 2, again the Néel-Arrhenius law is fitted to the measured dataset as shown in figure 9. For sample 2, the calculated values of T_a and f_o are 1449 K and 3.34×10^{17} Hz respectively. As these values seem implausibly high for the system under investigation, the results for sample 2 are likely being affected by the presence of a degree of interparticle interactions which have been reported to increase the f_0 of the system. The fittings hence imply that for sample 2 the interactions are not simply a perturbation to the anisotropy energy barriers, but are in fact strong in relation to the barrier height.

The strength of the dipolar interactions between nanoparticles will fall relative to the cube of the distance between the centres of the particles. The interaction strength between two adjacent particles is approximately given by μ^2/r^3, with μ being the average magnetic moment of the particles and r being the distance between the particles (Telem-Shafir and Markovich, 2005). One means of analysing the degree of interparticle interactions lies in analysing the widths of the normalised $\chi``$ curves. It has been reported that for an ensemble of non-interacting nanoparticles, the distribution of anisotropy energy barriers of the particles will typically determine the normalized width of the AC susceptibility versus temperature curves (Telem-Shafir and Markovich, 2005). The decrease in the scaled curve widths of the $\chi"$ curves of sample 2 relative to sample 1 are clearly visible in figure 10 for the 3 representative frequencies shown demonstrating that dipolar interactions are more prevalent in sample 2 than in sample 1. This seems to confirm the earlier conclusion from the Néel-Arrhenius model fitting to the sample 2 dataset. A further indication of the dipolar interaction strength lies in a comparison of the blocking temperatures of the

samples, which are expected to increase as the interactions strength increases. It is seen in figure 7 that the blocking temperatures for sample 2 are higher than those of sample 1 at similar frequencies. The reduced interactions from sample 1 may be related to the increased surface area of the particles which in turn may result in a thicker $Ni(OH)_2$ shell thus increasing the core interparticle distances.

To better quantify the effect of interparticle interactions the phenomenological Vogel-Fulcher law has been fitted to the experimental datasets of samples 1 and 2. For magnetically interacting particles, a Vogel-Fulcher law is used as a modification of the Arrhenius law but this is only valid for the case where the blocking temperature $>>T_0$. The law implies a characteristic ordering temperature T_0 which arises from the interactions within the system. If we consider the Vogel-Fulcher law and place $T_0 = 0$, then the Vogel-Fulcher law will simply reduce to the Arrhenius law implying a transition at $T_0 = 0K$. Previously, the Vogel-Fulcher law has also been successfully applied to spin glass type systems, where it can be used to account for the observed frequency dependence of the freezing temperature T_f. For the present superparamagnetic system, T_0 is the temperature at which the relaxation time would diverge, thus signalling a transition, the Vogel-Fulcher law is consequently only valid across a restricted temperature range and breaks down in the proximity of T_0. This law is reported to take the form $T_B=T_0+T_a/\ln(f_0/f_m)$ where T_0 measures the strength of the interparticle interactions. For the present systems under investigation $4.11x10^{11}$ Hz is taken as the likely magnitude of f_o. For sample 2, this model fitting as shown in figure 11 returns a value of 584 K for T_a and 14 K for $T_{0.}$ For sample 1, the value of T_a is 750K (close to the 747K returned by the Néel-Arrhenius law) with T_o being 0.17K (close to 0K), this shows the interparticle interactions to be negligible for sample 1 while remaining substantial for sample 2. The smaller value of T_a for sample

2 is to be expected given the smaller particle sizes of sample 2 relative to sample 1, thus helping to confirm the validity of the results.

Additionally, the parameter $\Phi = \Delta T_B/T_B\Delta\log_{10}f_m$ was calculated to examine the nature of the interparticle interactions. Here ΔT_B is the shift in the blocking temperature peak as determined from the χ'' curves, over the $\Delta\log_{10}f_m$ frequency interval (Goya et al., 2003, Dormann et al., 1988). In the present study the calculated value of Φ for sample 1 is 0.11 and is calculated to be 0.057 for sample 2. It has been reported that $0.05 < \Phi < 0.13$ for coupled nanoparticles with increasing values of Φ indicating a reduction in the coupling strength. For isolated nanoparticles, $\Phi = 0.13$ while for spin glasses Φ is reported to be very small (0.005-0.05).

The larger strength of interactions in sample 2 relative to sample 1 seems to imply a thicker $Ni(OH)_2$ shell around the metallic core. The sizes of the Ni nanoparticle cores could be anything up to the sizes identified using TEM microscopy depending on the $Ni(OH)_2$ layer thickness. It has been reported that for a system with cubic anisotropy and $K_1<0$, the value of K_a which is the effective uniaxial anisotropy is related to K_1 through the relation $K_a=K_1/12$ (Goya et al., 2003). If it is assumed that the value of K_1 for the system is actually the same as that of bulk Ni ($-8x10^5$ erg/cm^3) then using the equation ($T_a=K_aV/k_B$) and assuming spherical particles, we can back calculate the particle diameter for sample 1 to be 14.3nm. Since the TEM confirms the particle size to be ~32nm then this would suggest that approximately 9nm of the particle's radius is in fact OA and oxidised Ni in the form of $Ni(OH)_2$. For sample 2 a particle diameter of 13nm is estimated using this approach implying an approximate 0.5nm inter-core distance. It is known that anisotropies well above that of bulk Ni can become manifest in magnetic nanoparticle systems (Godsell et al., 2010) which would likely have the effect of reducing the particle diameter as calculated above. In spite of

this, it still becomes apparent that the quantity of $Ni(OH)_2$ present is considerably more substantial in sample 1 than in sample 2 leading to stronger interactions in sample 2 as evidenced in the magnetic measurements. The increased surface area of sample 1 would likely have led to an increased rate of oxygen diffusion through the OA capping layer thus leading to an increased rate of sub-capping layer surface oxidation of sample 1 relative to sample 2. Sub capping layer hydroxide shells of $Ni(OH)_2$ fabricated using this method may hence provide a convenient and facile means of controlling interparticle interactions in similar nanoparticle assemblages for differing applications.

IV Conclusions

$Ni/Ni(OH)_2$ core/shell nanoparticles have been shown to represent a potentially interesting nanomaterial. This morphology was observed to facilitate varying degrees of interparticle interactions within the nanoparticle assemblage. The presence of hydroxides within the material also leads to a more complex magnetic system with a combined antiferromagnetic/ferromagnetic signature. Static (DC) and dynamic (AC) magnetic properties of the synthesised samples were compared and the degree of interactions within the individual nanoparticle assemblages were investigated. The phenomenological Néel-Arrhenius and Vogel-Fulcher laws were successfully fitted to the experimental datasets to analyse the interparticle interaction strengths. A clear transition temperature peak was visible for both of the samples in the AC susceptibility as well as DC FC/ZFC measurements and was attributed to the antiferromagnetic $Ni(OH)_2$ corona around the metallic particle cores. The degree of oxidation of the Ni cores was also linked to the nanoparticle surface area. This implies that more accurate control of the hydroxide layer thickness is achievable which in turn

may facilitate a more precise control of the magnitude of interparticle interactions within similar nanocomposite assemblages.

Acknowledgements

This work was supported by Science Foundation Ireland (SFI) under the Principal Investigator Programme Contract No. SFI-PI-06/IN.1/I98 at the Tyndall National Institute. Additional funding was provided from the EU FP7 Network of Excellence (NoE) project - Beyond CMOS Nanodevices for Adding Functionalities to CMOS - 'NANOFUNCTION' (Grant No. 257375). Further support from SFI Grant No. 06/IN.1/I85 at the University of Limerick is additionally acknowledged.

Figure Captions

Figure 1: X-ray diffractograms of air dried Ni nanoparticles, peaks marked with a * correspond to the $Ni(OH)_2$ present in the systems.

Figure 2: TEM and HRTEM image of Sample 1 - 34nm.

Figure 3: TEM image of Sample 2 – bimodal 34/14nm particle size, .

Figure 4: Hysteresis curves for samples 1 and 2 at 10K, 30K and 300K, inset shows zoomed in image about the origin for the 10K measurements.

Figure 5: Reduced magnetisation curves (M/Ms) plotted as a function of Ms(H/T) for samples 1 and 2 inset shows zoomed in image about the origin for the measurements.

Figure 6: Loop Shift measurements for samples 1 and 2, inset shows zoomed in image about the origin.

Figure 7: Temperature variation of $\chi`$ and $\chi``$ for samples 1 and 2.

Figure 8: Field-Cooled and Zero-Field-Cooled curves for samples 1 and 2 with 1 Oe applied field strength. Inset of 8(b) shows Field-Cooled and Zero-Field-Cooled curves for sample 2 with 10Oe applied field strength.

Figure 9: Néel-Arrhenius model fitting to the blocking temperatures obtained from the χ'' dataset peaks for sample 1 and sample 2.

Figure 10: Scaled χ'' vs temperature for samples 1 and 2 at varying frequencies.

Figure 11: Vogel-Fulcher model fitting to the blocking temperatures from the χ'' dataset for sample 2.

412

413

Figure 1 : J. Godsell et al.

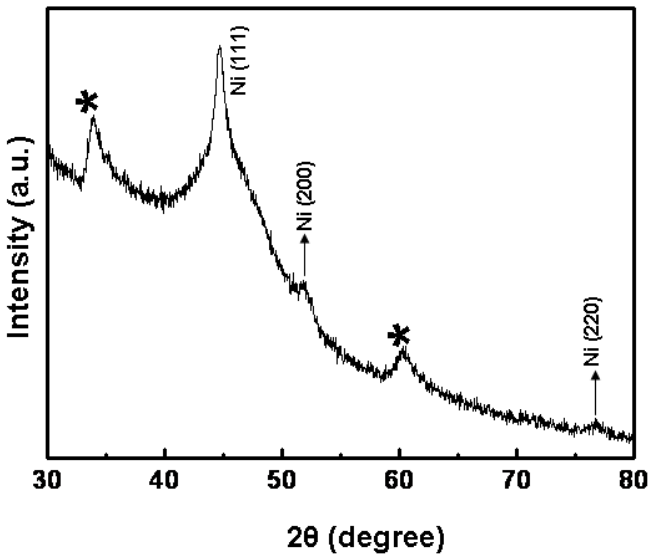

Figure 2: J. Godsell et al.

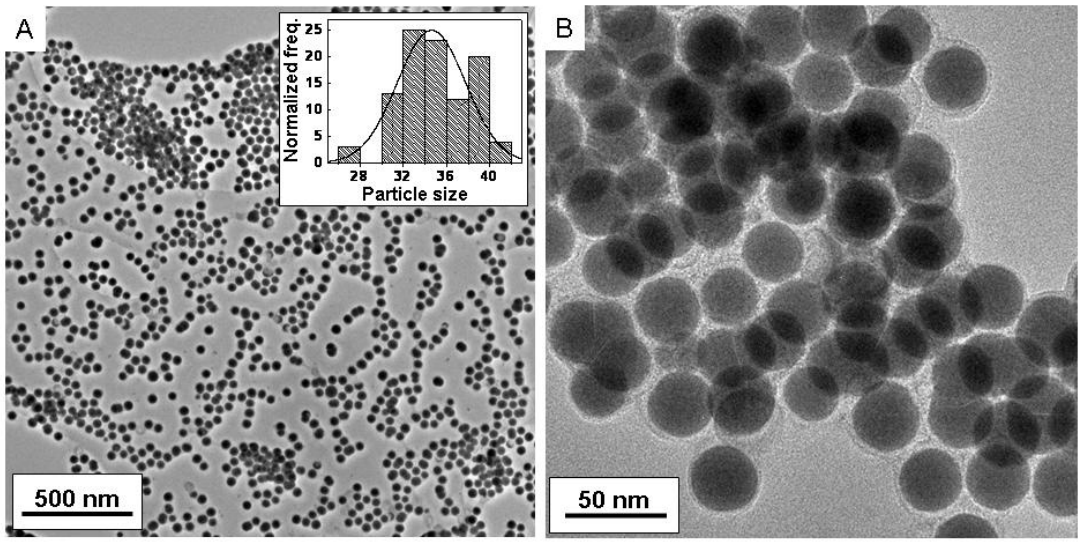

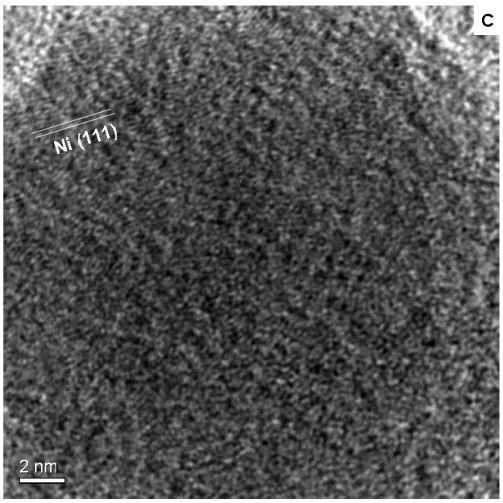

Figure 3 : J. Godsell et al.

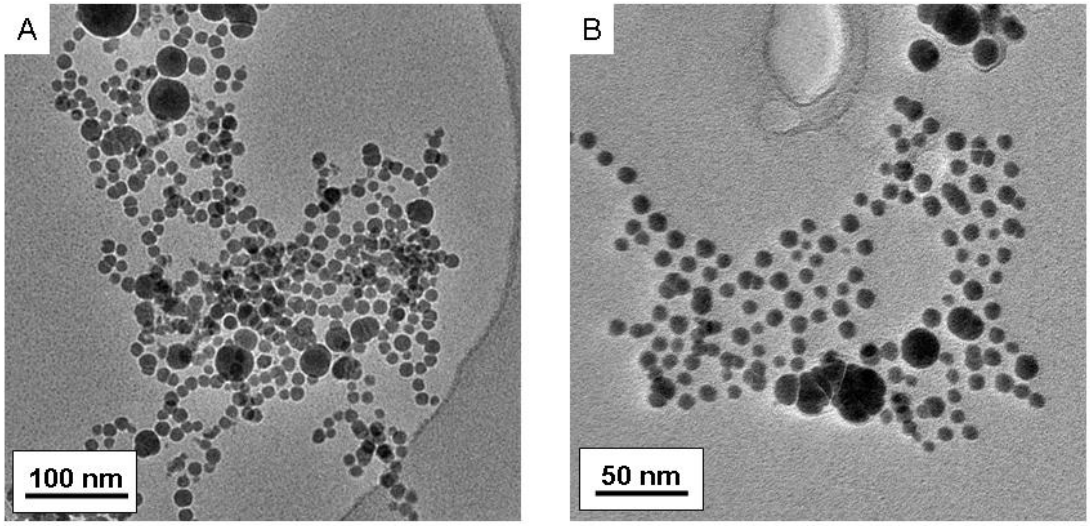

Figure 4 : J. Godsell et al.

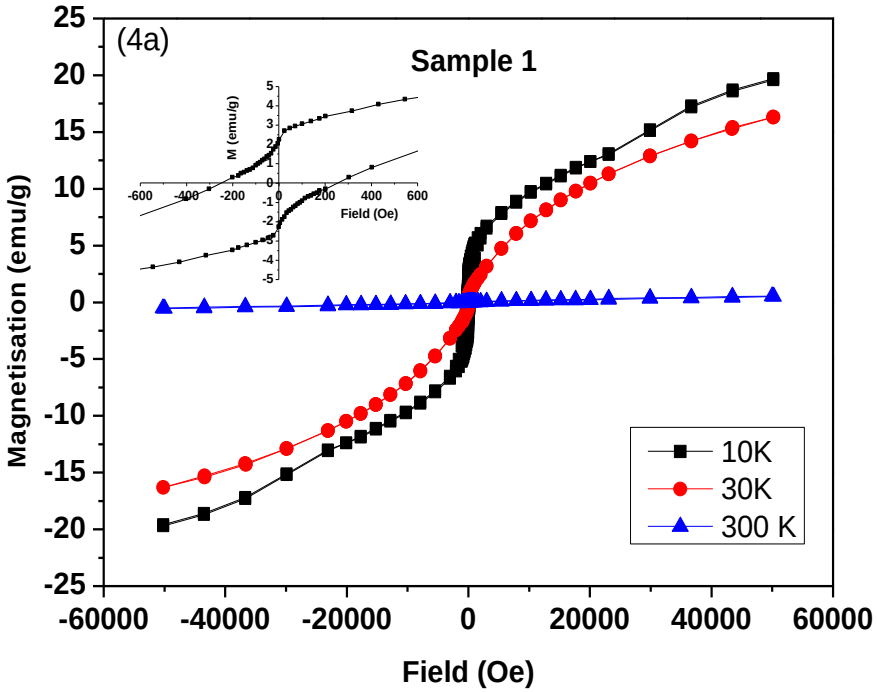

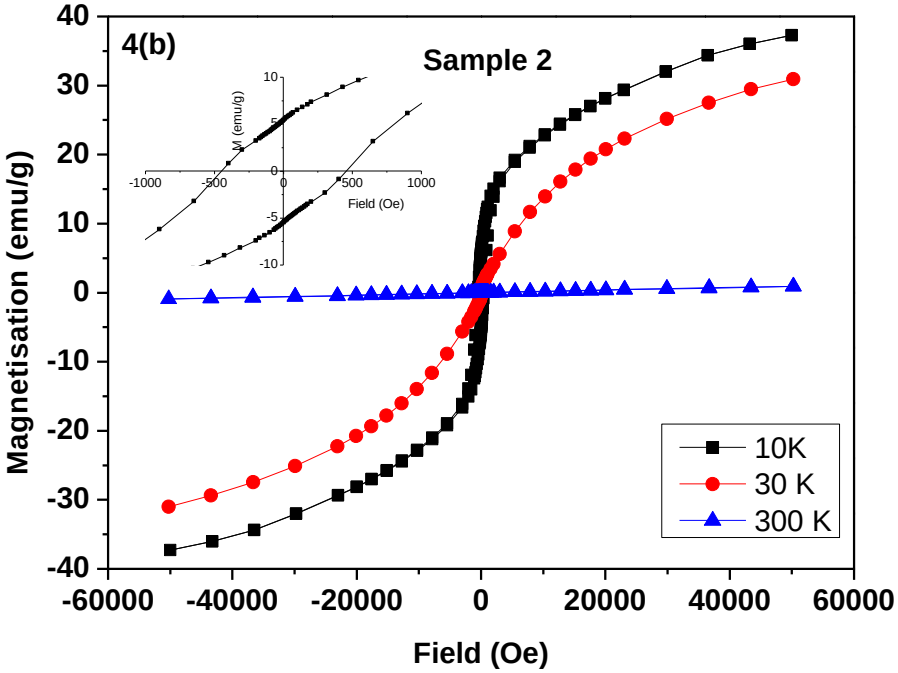

445 **Figure 5 : J. Godsell et al.**

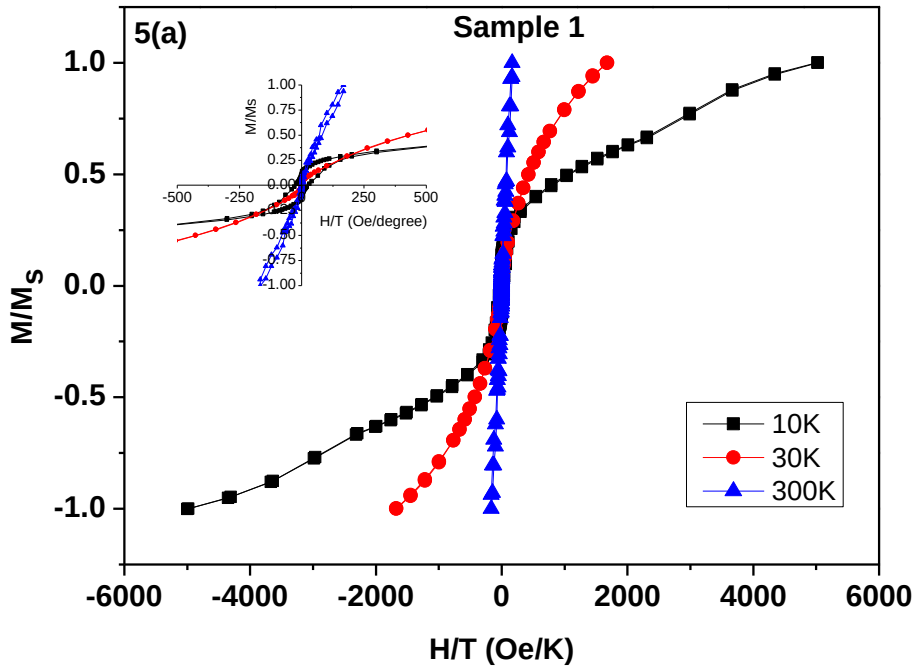

446

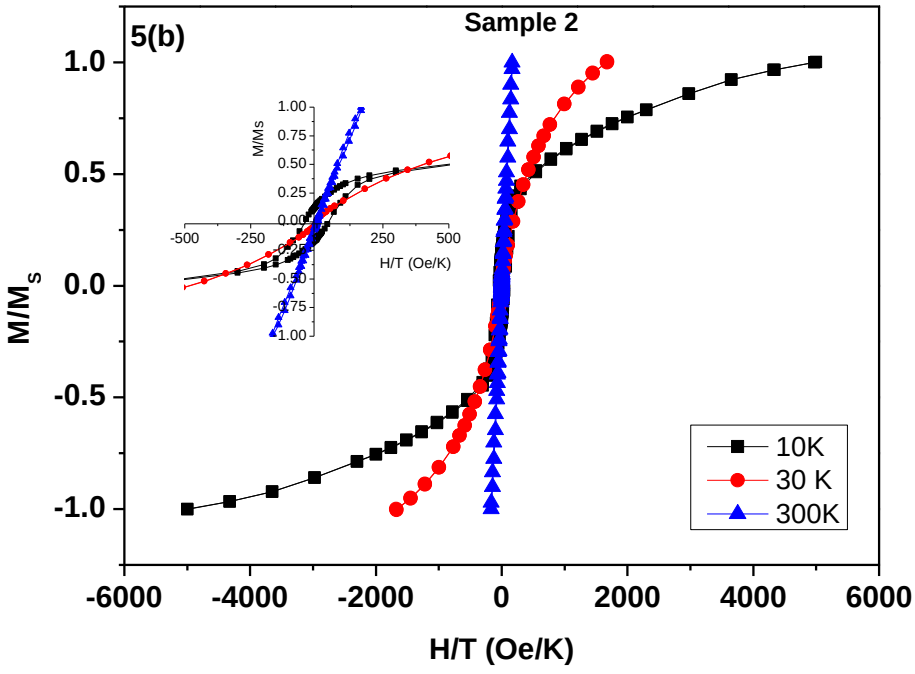

447
448
449
450

451

452

453 **Figure 6 : J. Godsell et al.**

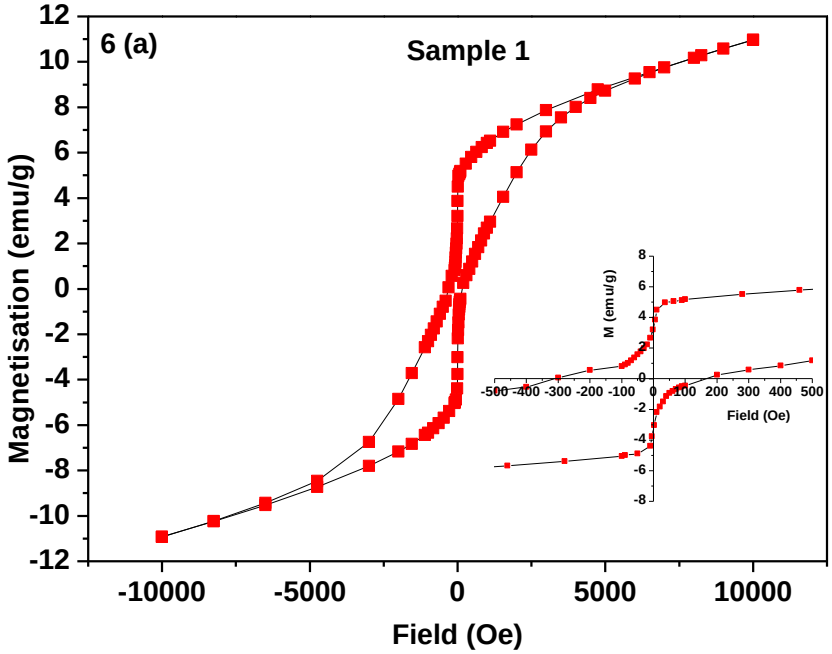

454

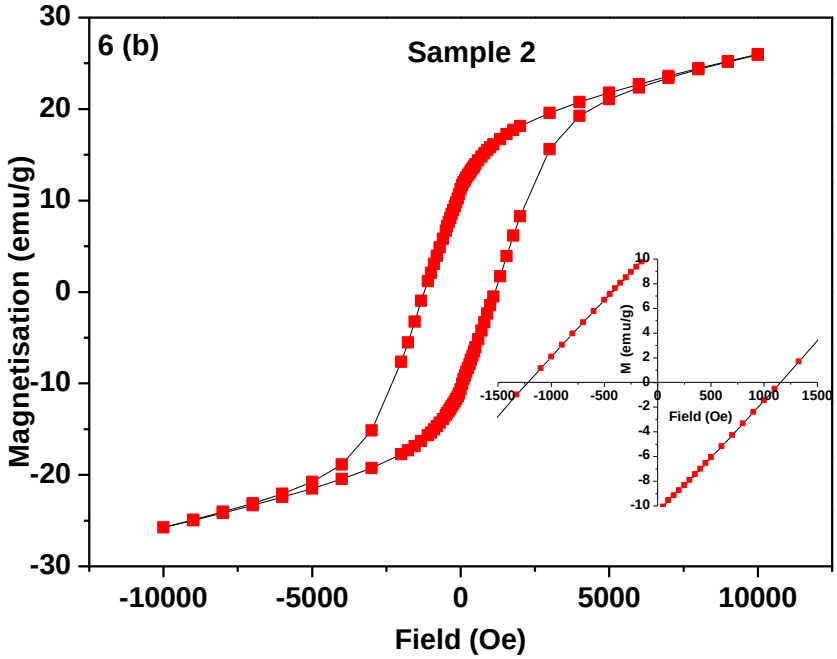

455

Figure 7 : J. Godsell et al.

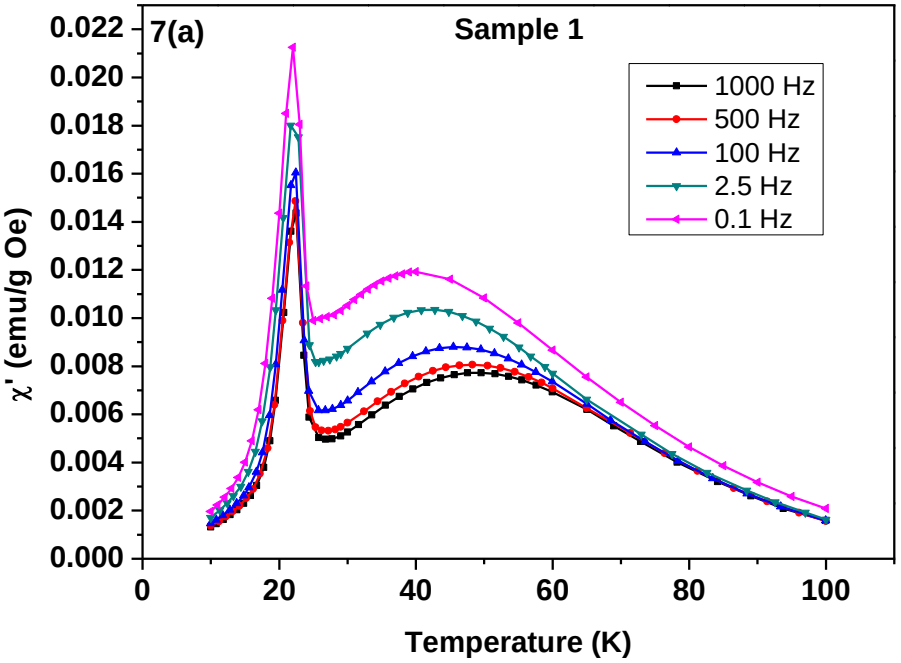

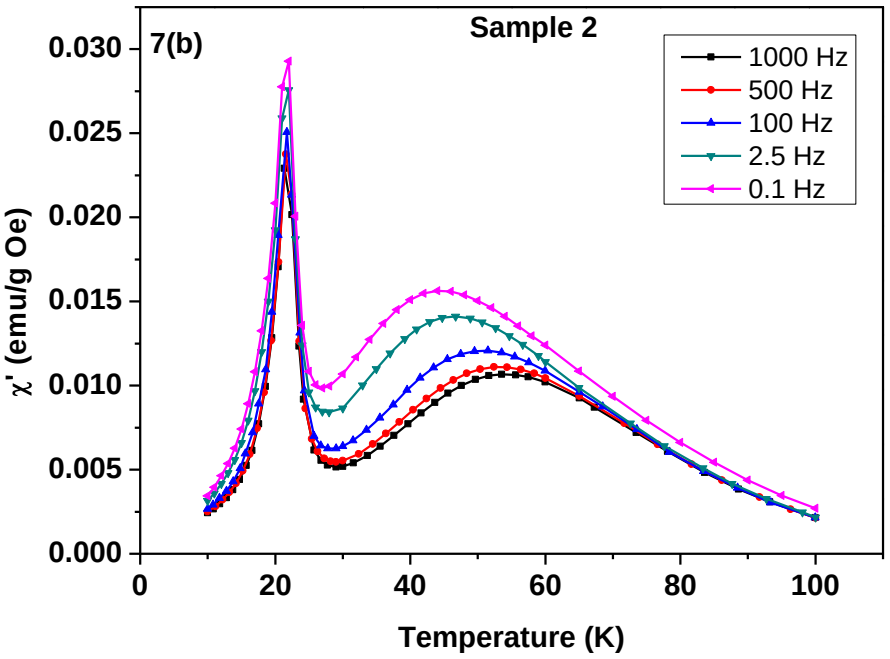

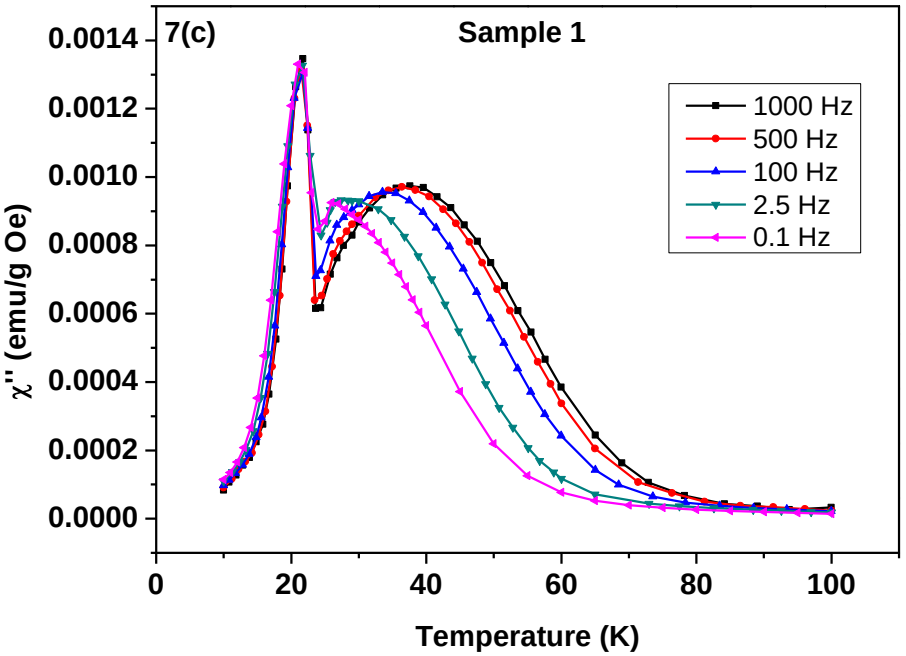
7(c)
Sample 1
1000 Hz
500 Hz
100 Hz
2.5 Hz
0.1 Hz
χ'' (emu/g Oe)
Temperature (K)
0.0014
0.0012
0.0010
0.0008
0.0006
0.0004
0.0002
0.0000
0
20
40
60
80
100

461

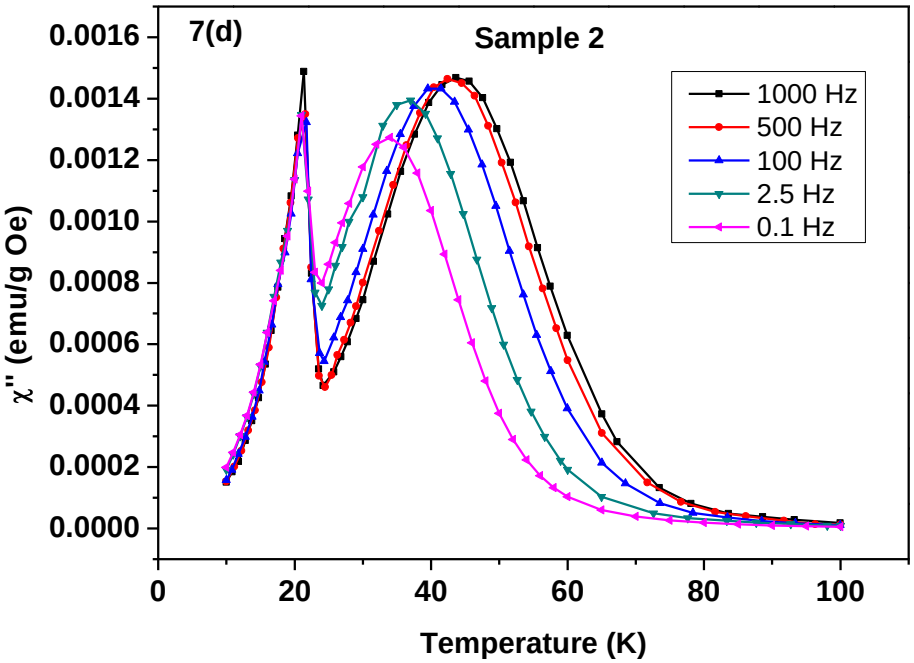
7(d)
Sample 2
1000 Hz
500 Hz
100 Hz
2.5 Hz
0.1 Hz
χ'' (emu/g Oe)
Temperature (K)
0.0016
0.0014
0.0012
0.0010
0.0008
0.0006
0.0004
0.0002
0.0000
0
20
40
60
80
100

462

463

464 **Figure 8: J. Godsell et al.**

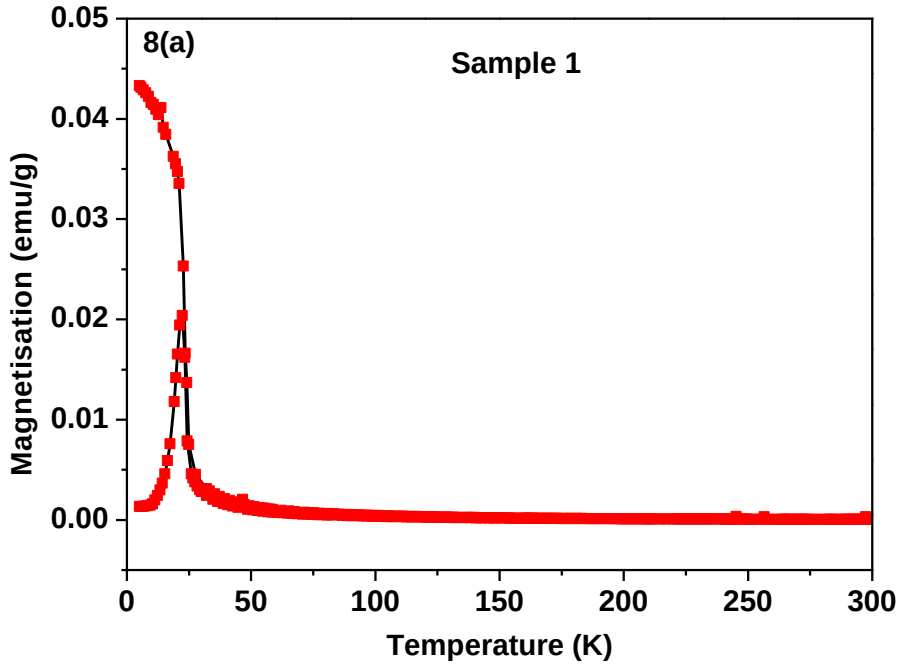

465

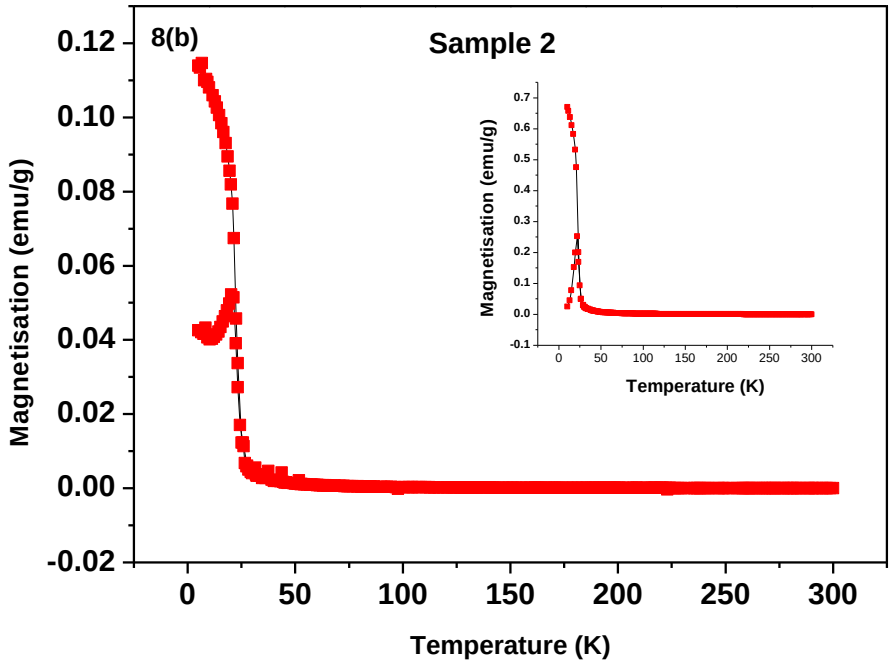

466

467

468

469

470 **Figure 9 : J. Godsell et al.**

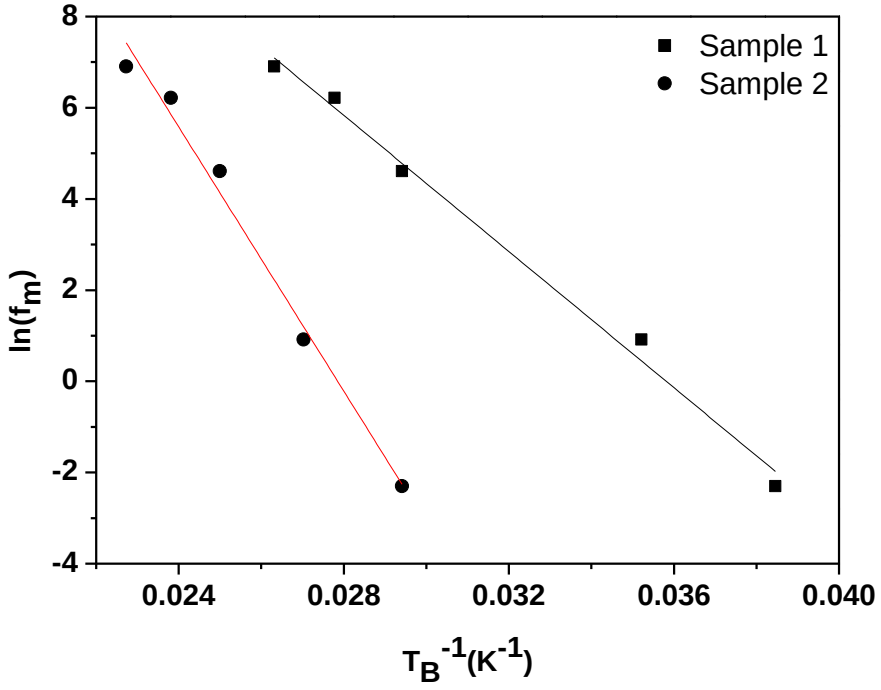

471

472

473 **Figure 10 : J. Godsell et al.**

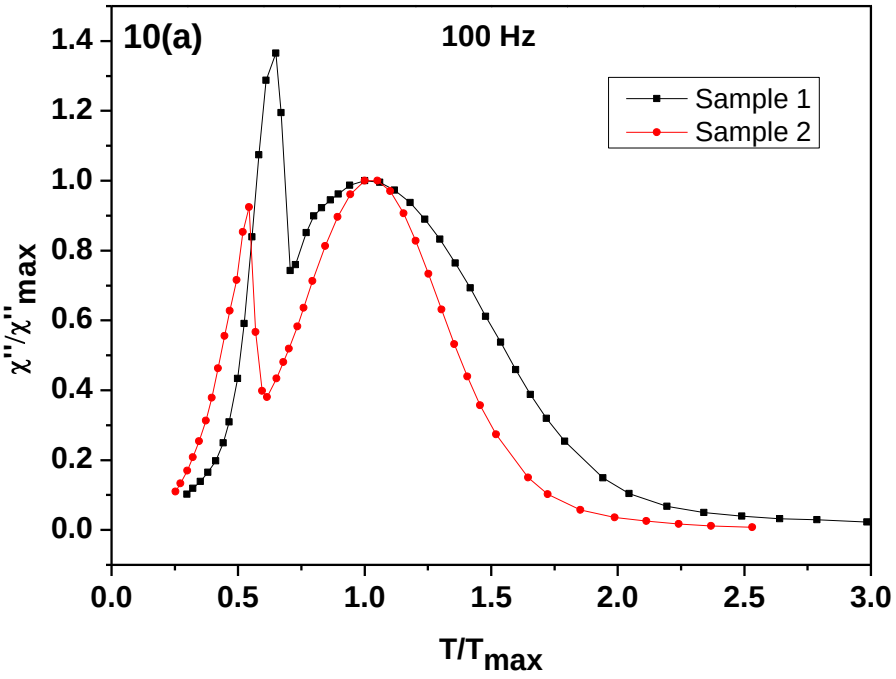

474
475

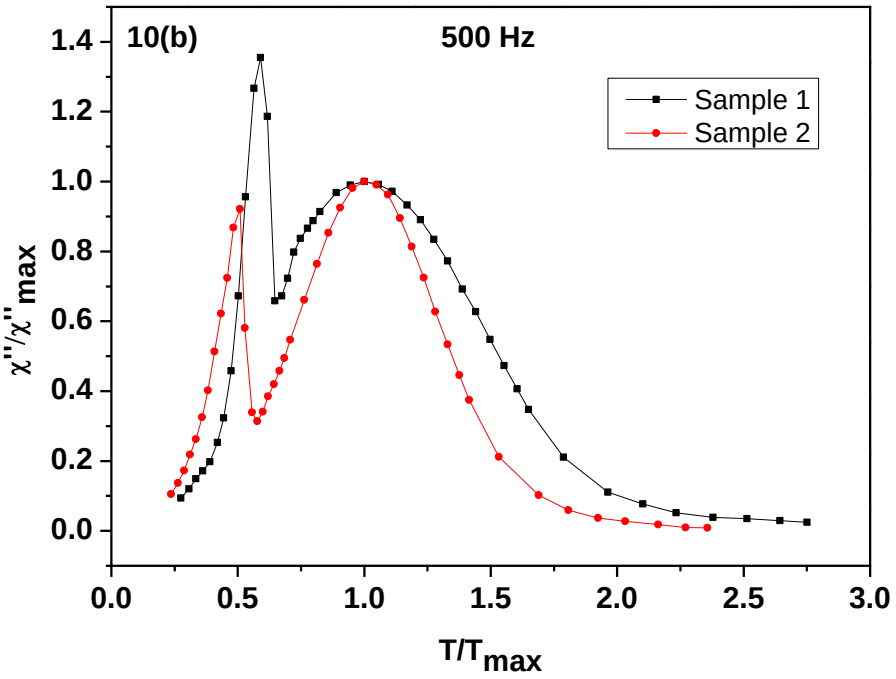

476
477

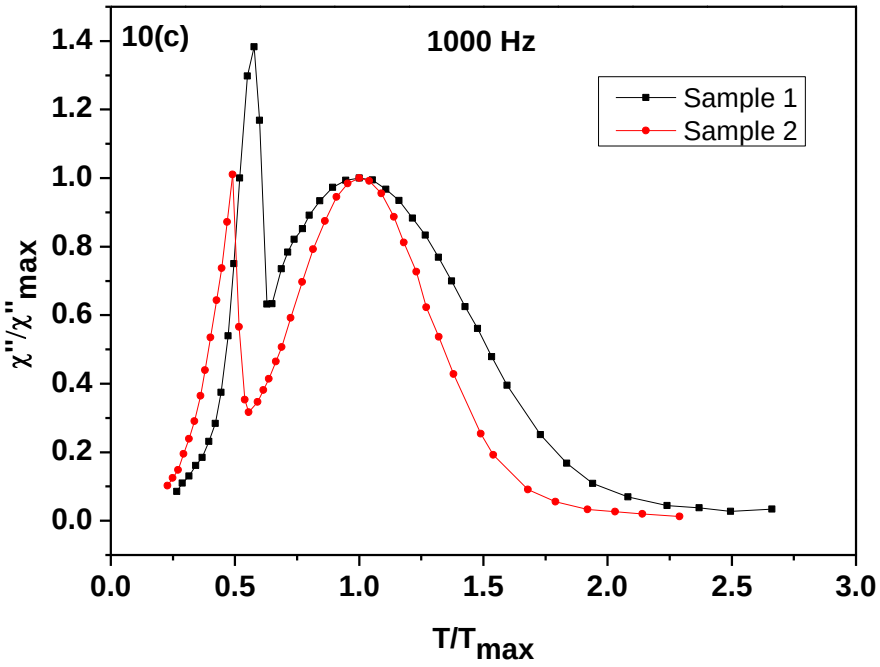

478

479

480

481

Figure 11 : J.Gosdell et al.

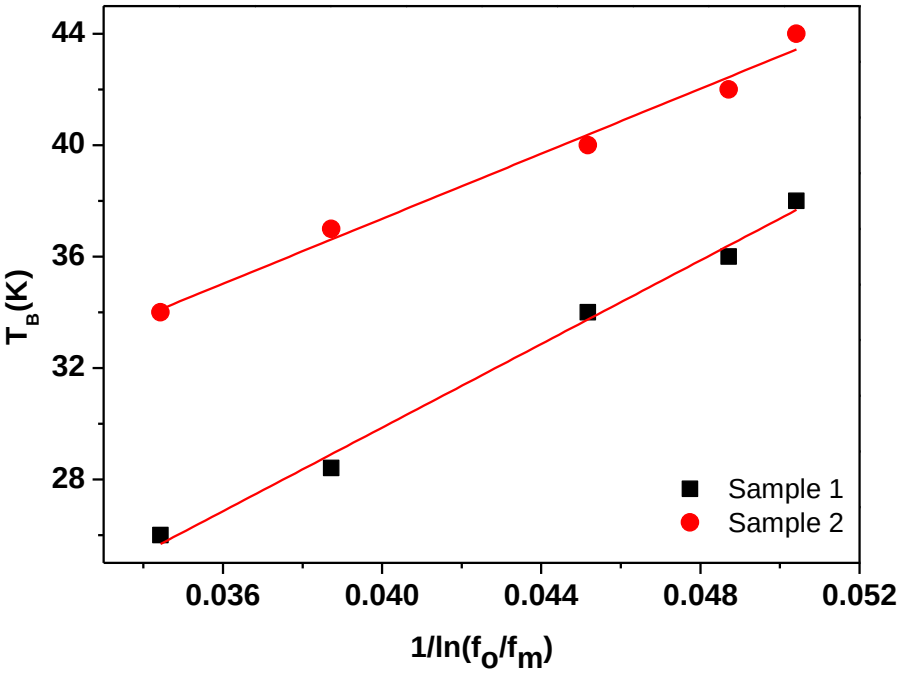

References

AC susceptibility, Introduction by Dinesh Martien, Quantum Design Application Note. .

ACET, M., DUMAN, E., WASSERMANN, E. F., MANOSA, L. & PLANES, A. 2002. Coexisting ferro- and antiferromagnetism in Ni[sub 2]MnAl Heusler alloys. ***Journal of Applied Physics,*** **92, 3867-3871.**

BALA, T., GUNNING, R. D., VENKATESAN, M., GODSELL, J. F., ROY, S. & RYAN, K. M. 2009. Block copolymer mediated stabilization of sub-5 nm superparamagnetic nickel nanoparticles in an aqueous medium. ***Nanotechnology,*** **20, 415603**

BANERJEE, S., ROY, S., CHEN, J. W. & CHAKRAVORTY, D. 2000. Magnetic properties of oxide-coated iron nanoparticles synthesized by electrodeposition. ***Journal of Magnetism and Magnetic Materials,*** **219, 45-52.**

BEDANTA, S. & KLEEMANN, W. 2009. Supermagnetism. ***Journal of Physics D-Applied Physics,*** **42.**

DAS, D., ROY, S., CHEN, J. W. & CHAKRAVORTY, D. 2002. Interface controlled electrical and magnetic properties in Fe-Fe3O4-silica gel nanocomposites. ***Journal of Applied Physics,*** **91, 4573-4579.**

DONEGAN, K. P., GODSELL, J. F., TOBIN, J. M., O'BYRNE, J. P., OTWAY, D. J., MORRIS, M. A., ROY, S. & HOLMES, J. D. 2011. Microwave-assisted synthesis of icosahedral nickel nanocrystals. ***CrystEngComm,*** **13, 2023.**

DORMANN, J. L., BESSAIS, L. & FIORANI, D. 1988. A DYNAMIC STUDY OF SMALL INTERACTING PARTICLES - SUPERPARAMAGNETIC MODEL AND SPIN-GLASS LAWS. ***Journal of Physics C-Solid State Physics,*** **21, 2015-2034.**

DUMAN, E., ACET, M., ELERMAN, Y., ELMALI, A. & WASSERMANN, E. F. 2002. Magnetic interactions in Pr1-xTbxMn2Ge2. ***Journal of Magnetism and Magnetic Materials,*** **238, 11-21.**

GITTLEMAN, J. I., ABELES, B. & BOZOWSKI, S. 1974. Superparamagnetism and relaxation effects in granular Ni-SiO_{2} and Ni-Al_{2}O_{3} films. ***Physical Review B,*** **9, 3891.**

GODSELL, J. F., DONEGAN, K. P., TOBIN, J. M., COPLEY, M. P., RHEN, F. M. F., OTWAY, D. J., MORRIS, M. A., O'DONNELL, T., HOLMES, J. D. & ROY, S. 2010. Magnetic properties of Ni nanoparticles on microporous silica spheres. ***Journal of Magnetism and Magnetic Materials,*** **322, 1269-1274.**

GOMES, J. D. A., SOUSA, M. H., TOURINHO, F. A., AQUINO, R., DA SILVA, G. J., DEPEYROT, J., DUBOIS, E. & PERZYNSKI, R. 2008. Synthesis of Core−Shell Ferrite Nanoparticles for Ferrofluids: Chemical and Magnetic Analysis. ***The Journal of Physical Chemistry C,*** **112, 6220-6227.**

GONG, W., LI, H., ZHAO, Z. & CHEN, J. 1991. Ultrafine particles of Fe, Co, and Ni ferromagnetic metals. ***Journal of Applied Physics,*** **69, 5119-5121.**

GOYA, G. F., FONSECA, F. C., JARDIM, R. F., MUCCILLO, R., CARRENO, N. L. V., LONGO, E. & LEITE, E. R. 2003. Magnetic dynamics of single-domain Ni nanoparticles. ***Journal of Applied Physics,*** **93, 6531-6533.**

HUH, Y.-M., JUN, Y.-W., SONG, H.-T., KIM, S., CHOI, J.-S., LEE, J.-H., YOON, S., KIM, K.-S., SHIN, J.-S., SUH, J.-S. & CHEON, J. 2005. In

Vivo Magnetic Resonance Detection of Cancer by Using Multifunctional Magnetic Nanocrystals. ***Journal of the American Chemical Society,*** **127, 12387-12391.**

JORDAN, A., SCHOLZ, R., WUST, P., FÄHLING, H. & ROLAND, F. 1999. Magnetic fluid hyperthermia (MFH): Cancer treatment with AC magnetic field induced excitation of biocompatible superparamagnetic nanoparticles. ***Journal of Magnetism and Magnetic Materials,*** **201, 413-419.**

KNOBEL, M., NUNES, W. C., SOCOLOVSKY, L. M., DE BIASI, E., VARGAS, J. M. & DENARDIN, J. C. 2008. Superparamagnetism and other magnetic features in granular materials: A review on ideal and real systems. ***Journal of Nanoscience and Nanotechnology,*** **8, 2836-2857.**

LEE, I. S., LEE, N., PARK, J., KIM, B. H., YI, Y.-W., KIM, T., KIM, T. K., LEE, I. H., PAIK, S. R. & HYEON, T. 2006. Ni/NiO Core/Shell Nanoparticles for Selective Binding and Magnetic Separation of Histidine-Tagged Proteins. ***Journal of the American Chemical Society,*** **128, 10658-10659.**

LI, Z. L., GODSELL, J. F., O'BYRNE, J. P., PETKOV, N., MORRIS, M. A., ROY, S. & HOLMES, J. D. 2010. Supercritical Fluid Synthesis of Magnetic Hexagonal Nanoplatelets of Magnetite. ***Journal of the American Chemical Society,*** **132, 12540-12541.**

LU, A.-H., SALABAS, E. L. & SCHÜTH, F. 2007. Magnetic Nanoparticles: Synthesis, Protection, Functionalization, and Application. ***Angewandte Chemie International Edition,*** **46, 1222-1244.**

MCGILL, S. L., CUYLEAR, C. L., ADOLPHI, N. L., OSINSKI, M. & SMYTH, H. D. C. 2009. Magnetically Responsive Nanoparticles for Drug Delivery Applications Using Low Magnetic Field Strengths. ***Ieee Transactions on Nanobioscience,*** **8, 33-42.**

OSAKA, T., IIDA, H., TOMINAKA, S. & HACHISU, T. 2008. New Trends in Nanoparticles: Syntheses and Their Applications to Fuel Cells, Health Care, and Magnetic Storage. ***Israel Journal of Chemistry,*** **48, 333-347.**

SHIM, H., MANIVANNAN, A., SEEHRA, M. S., REDDY, K. M. & PUNNOOSE, A. 2006. Effect of interparticle interaction on the magnetic relaxation in NiO nanorods. ***Journal of Applied Physics,*** **99, 08Q503.**

SINGH, V., SEEHRA, M. S. & BONEVICH, J. 2008. Nickel-silica nanocomposite: Variation of the blocking temperature with magnetic field and measuring frequency. ***Journal of Applied Physics,*** **103, 07D524.**

SINGH, V., SEEHRA, M. S. & BONEVICH, J. 2009. ac susceptibility studies of magnetic relaxation in nanoparticles of Ni dispersed in silica. ***Journal of Applied Physics,*** **105, 07B518.**

SKUMRYEV, V., STOYANOV, S., ZHANG, Y., HADJIPANAYIS, G., GIVORD, D. & NOGUES, J. 2003. Beating the superparamagnetic limit with exchange bias. ***Nature,*** **423, 850-853.**

SPELIOTIS, D. E. 1999. Magnetic recording beyond the first 100 Years. ***Journal of Magnetism and Magnetic Materials,*** **193, 29-35.**

SUBBAIAH, T., MOHAPATRA, R., MALLICK, S., MISRA, K. G., SINGH, P. & DAS, R. P. 2003. Characterisation of nickel hydroxide precipitated from solutions containing Ni2+ complexing agents. ***Hydrometallurgy,*** **68, 151-157.**

SUZUKI, M., SUZUKI, I. S. & ENOKI, T. 2000. Spin-glass phase and re-entrant spin-glass phase in diluted three-dimensional Ising antiferromagnet NicMg1-c(OH)(2). ***Journal of Physics-Condensed Matter,*** **12, 1377-1397.**

TELEM-SHAFIR, T. & MARKOVICH, G. 2005. Magnetization dynamics in arrays of strongly interacting magnetic nanocrystals. ***Journal of Chemical Physics,*** **123, 204715.**